A comparison of impulse response modification techniques for time reversal with application to crack detection

Sarah M. Young, Brian E. Anderson, Matthew L. Willardson, Paige E. Simpson, and Pierre-Yves Le Bas

Citation: The Journal of the Acoustical Society of America **145**, 3195 (2019); doi: 10.1121/1.5109395
View online: https://doi.org/10.1121/1.5109395
View Table of Contents: https://asa.scitation.org/toc/jas/145/5
Published by the Acoustical Society of America

A comparison of impulse response modification techniques for time reversal with application to crack detection

Sarah M. Young,[1] Brian E. Anderson,[1,a)] Matthew L. Willardson,[1] Paige E. Simpson,[1] and Pierre-Yves Le Bas[2]

[1]*Acoustics Research Group, Department of Physics and Astronomy, Brigham Young University, N283 Eyring Science Center, Provo, Utah 84602, USA*

[2]*Detonator Technology (Q-6), Los Alamos National Laboratory, MS D446, Los Alamos, New Mexico 87545, USA*

(Received 29 January 2019; revised 9 April 2019; accepted 7 May 2019; published online 31 May 2019)

Time reversal (TR) focusing used for nonlinear detection of cracks relies on the ability of the TR process to provide spatially localized, high-amplitude excitation. The high amplitude improves the ability to detect nonlinear features that are a signature of the motion of closed cracks. It follows that a higher peak focal amplitude than what can be generated with the traditional TR process will improve the detection capability. Modifying the time-reversed impulse response to increase the amplitude of later arrivals in the impulse response, while maintaining the phase information of all arrivals, increases the overall focal signal amplitude. A variety of existing techniques for increasing amplitude are discussed, and decay compensation TR, a technique wherein amplitude is increased according to the inverse of the amplitude envelope of the impulse response decay, is identified as the best modification technique for nonlinear crack detection. This technique increases the focal signal amplitude with a minor introduction of harmonic content, a drawback in two other methods studied, one-bit TR and clipping TR. A final study employs both decay compensation TR and traditional TR, focusing on a rod with stress corrosion cracking, and compares the merits of each in detecting nonlinearity from cracks in a real system. © *2019 Acoustical Society of America*.
https://doi.org/10.1121/1.5109395

[JDR] Pages: 3195–3207

I. INTRODUCTION

The time reversal (TR) process utilizes the impulse response of a system, between a source and a receiver, to generate both a spatial and temporal focus of energy at a chosen location.[1,2] The impulse response is reversed in time and then emitted by the source (reciprocal TR[2]) with the low-amplitude vibrations emitted first and the high-amplitude vibrations last. The timing of the emitted waves is determined by the reversed impulse response (RIR). For a time-invariant system, each of the emitted waves travels along the paths traversed during the impulse response measurement, and the timing is such that energy from each emission arrives simultaneously at the receiver location, creating a constructive focusing of energy that is generally impulsive in nature.

The TR focus of energy has been utilized for nondestructive evaluation (NDE; i.e., crack localization) since the early 1990s, for example, with Chakroun *et al.* using TR to locate scatterers in a solid sample submerged in a fluid.[3,4] In 2001, Guyer first proposed using high-amplitude TR focusing for nonlinear imaging of cracks,[5] and Ulrich *et al.* demonstrated this experimentally a few years later by locating a surficial crack in a doped glass sample.[6] Studies since then have used TR to find nonlinearity in various types of surface cracks,[7–10] near-surficial cracks and delaminations,[10,11] and even buried cracks.[10,12] The detection of cracks using nonlinear methods is rooted in the premise that cracks will generate nonlinear frequency mixing when excited with sufficient amplitude.[13,14] It has been shown that nonlinear methods detect damage sooner than their linear counterparts.[15] TR focusing at a damaged location results in the generation of higher harmonic frequency content. Thus, nonlinear detection methods require a high signal-to-noise ratio (SNR) such that higher-order harmonics are not buried in the noise floor.[16] While TR focusing inherently generates high-amplitude energy focusing, traditional TR signal processing may not be the optimal technique for nonlinear detection of cracks in otherwise isotropic media. A review of the use of TR techniques to detect nonlinear acoustic features for nondestructive evaluation was recently published by Anderson *et al.*[17]

Modifications to traditional TR processing have been studied in a variety of contexts. One-bit TR was developed by Derode *et al.* as a method of increasing the amplitude of TR focusing, a technique later explored for use in lithotripsy.[18,19] Others have used similar techniques wherein the instantaneous amplitude of the impulse response as time progresses is increased to compensate for the natural decay from geometric spreading losses and propagation losses in attenuating media, thereby increasing the SNR of an impulse response in strongly attenuating media.[20,21] Deconvolution TR, or inverse filtering, was introduced as a means of compensating for resonances in the impulse response to optimize the impulsive nature of a TR focus of energy.[22,23] Studies have examined the reliance of focal amplitude on the length

a)Electronic mail: bea@byu.edu

of the initial pulse (i.e., the bandwidth).[24–26] Physical system adjustments have sought to increase SNR through other means such as the introduction of a chaotic cavity[27–30] or the use of an acoustic metamaterial-based filter.[31] Recently, Willardson *et al*. published experimental research manipulating TR processing in order to maximize the focal amplitude of audible sound in a reverberation chamber.[21]

The work by Willardson *et al*. experimentally compared five different techniques that adjust the RIR to ultimately determine which provided the highest peak focal amplitude. The study was conducted in a reverberation chamber using a loudspeaker and a microphone, constituting a wide bandwidth system, and examined various attributes of the focal signals, including peak focal amplitude and temporal quality. While this study was valuable for a thorough understanding of TR in air, the study may not contribute information relevant to crack detection in a solid with a fairly resonant system, as is common for NDE experiments. This paper includes frequency analysis of higher harmonic generation and an evaluation of the spatial quality of the TR focusing, something that Willardson *et al*. did not explore.

While previous research has successfully developed modifications of RIR signal processing techniques based on specific targeted outcomes, a comparison of each of these modification techniques with application to NDE has not been done, nor have the impacts of these techniques on the introduction of harmonic frequency content been quantified (many of these techniques are inherently nonlinear processes). Typical solutions for generating the necessarily high SNR in focal signals used in crack detection can require the use of many generation channels or signal amplification beyond the linear limits of the system. The ideal solution to maximize SNR would maintain the physical system but optimize available amplification through the processing of the RIR(s) to increase excitation amplitude at the focus without unduly introducing noise at higher harmonic frequencies or undermining the benefits of using TR for nonlinear crack detection (i.e., spatially compressed focusing).

The objective here is to determine the TR signal processing technique that delivers the largest peak focal amplitude in conjunction with the best temporal quality, a spatially confined focus, and low higher harmonic generation. The purpose of this paper is to experimentally compare five different TR signal processing techniques: deconvolution TR, one-bit TR, clipping TR, decay compensation TR, and as a benchmark, traditional TR, to determine the processing technique best suited for detection of cracks using nonlinear analyses. In this study, it is found that decay compensation TR is the optimal choice for the highest focal amplitude coupled with low higher harmonic generation. It is then shown that decay compensation TR is less susceptible to noise and false detections than traditional TR in the detection of cracks.

The remainder of the paper first describes the experimental setup followed by a description of each of the TR techniques explored. This is followed by a description of the analysis metrics used to compare the methods, peak focal amplitude, temporal quality, spatial quality, and fundamental to higher harmonic ratios. The results are presented for all the TR techniques tested, with some techniques tested with different applied thresholds. Finally, a study is presented that compares the use of traditional and decay compensation TR to find stress corrosion cracking (SCC) in a steel rod.

The nonlinear NDE of cracks and defects using TR is usually accomplished through the detection of a relative increase in harmonics[8,11,32] or sum and difference frequencies[6,7] (i.e., through the introduction of nonlinear frequency content). Some techniques have been developed to detect distortions in the focal signal when the focusing experiment is conducted multiple times. Phase inversion is one of these techniques where the RIR(s) are broadcast as usual and then are phase inverted by 180°, and these inverted RIR(s) are then broadcast and differences in the two focal signals are compared since for linear focusing these signals should be identical other than a 180° phase shift.[11] Another variant of phase inversion is the third-order phase symmetry analysis technique in which RIR(s) are broadcast with phases of 0°, 120°, and 240°, and the resulting focal signals are combined in different ways to determine changes to the fundamental frequency, even harmonics, and odd harmonics.[33] Finally, the scaling subtraction method utilizes RIR(s) that are intentionally broadcast at different amplification levels to create low- and high-amplitude focal signals, which should scale linearly if the focusing is a linear process.[8,34–36] Each of these techniques is designed to make it easier to detect increases in nonlinear frequency content due to the presence of cracks or defects. Finally, there are many metrics that have been developed to quantify distortions in the focal signals due to the presence of the harmonics. For example, if phase inversion is used, the 0° and 180° focal signals are added together. Any residual energy in this summed signal is considered to be generated by the crack or defect, so this residual signal might be squared and summed around the focal time as a quantifiable metric to detect a crack or defect. Young *et al*.[32] normalized the spectra of the focal signals according to the energy contained in the fundamental frequency bandwidth, and then summed the energy contained in the second harmonic bandwidth to produce a nonlinear metric. The present paper does not explore how each of the TR signal processing techniques impacts each of these nonlinearity detection techniques. Instead, the ratio of the second harmonic to the fundamental frequency and the ratio of the third harmonic to the fundamental frequency are used to compare the nonlinearities generated by the signal processing applied to the RIR(s) in results obtained on a linear, intact sample. Then, the nonlinearity detection technique used by Young *et al*. is employed to compare traditional TR and decay compensation TR on a cracked sample.

II. TR AND EXPERIMENTAL SETUP

The TR process consists of two steps, a forward step, and a backward step. The forward step consists of finding impulse responses from one or more sources to one or more receivers. Typically, an impulse is broadcast from each source and the response is recorded with each receiver to obtain the impulse response(s). In the backward step of the traditional TR process, each impulse response is simply

reversed in time and emitted from the receiver. In a variation called reciprocal TR, the RIRs are broadcast from the original source locations, generating a focus of energy at the receiver location(s).[2]

For the experiments described in this paper, a different method is utilized to obtain the impulse responses. First, the broadcast of a true impulsive signal is difficult, from a practical standpoint, for finite-bandwidth transducers. These emissions typically generate low-amplitude waves, meaning the SNR of the impulse response is poor. Instead a finite-bandwidth, a linear chirp signal is used as the source signal, an example of which is shown in Fig. 1(a). The chirp signal broadcast, being band limited, is efficiently broadcast from transducers and therefore it affords a higher SNR recording than the recording of the response to an impulsive broadcast. The chirp response is recorded by the receiver and is then cross correlated with the original chirp signal as an approximate means to obtain the impulse response [see Figs. 1(b) and 1(c)].[37,38] The impulse response is then reversed in time [Fig. 1(d)] and is broadcast from the same source as the chirp signal (reciprocal TR). The TR focus, shown in Fig. 1(e), occurs at the receiver. This allows the source transducers to be bonded in place, and a focus of energy may be generated wherever the receiver is placed.

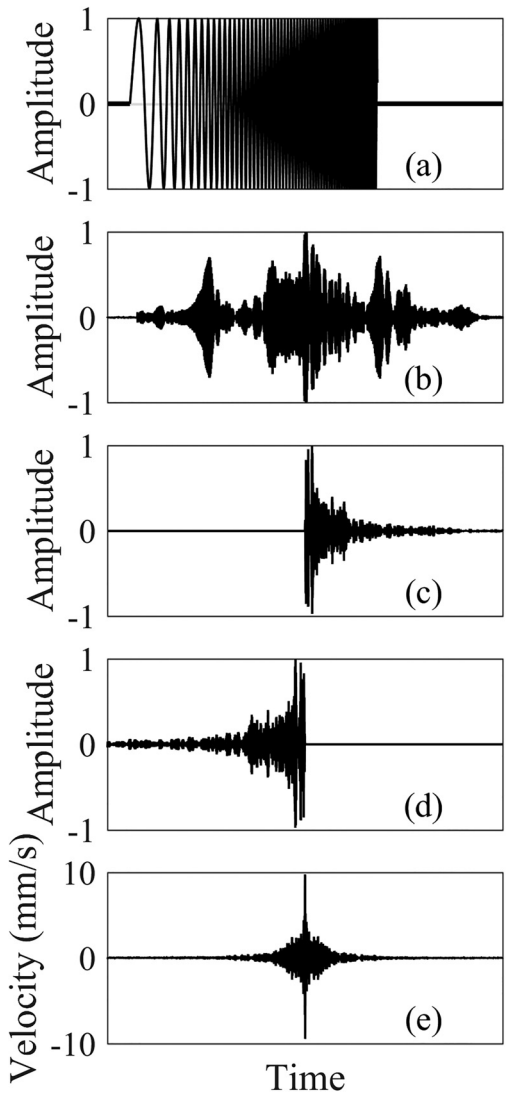

FIG. 1. Example signals used in the TR process. Except for (e), the amplitudes are normalized and in arbitrary units. (a) Source chirp (with frequencies altered for visualization), (b) chirp response, (c) impulse response, (d) RIR, (e) focal signal.

The experimental setup, depicted in Fig. 2, is comprised of a steel disk measuring 20.2 cm (8 in) in diameter and 2.5 cm (1 in) in thickness, which is elevated by three rubber stoppers 2 cm (0.8 in) above an optical table. A piezoelectric transducer (APC International, Mackeyville, PA), material type 850, with diameter 19 mm and thickness 9.5 mm, is epoxied to one side of the disk and operates as the source in both the forward and backward propagation steps. The steel disk is placed with the piezoelectric facing downward toward the table. A PSV-400 Polytec (Waldbronn, Germany) scanning laser Doppler vibrometer (SLDV), a noncontact and mobile receiver, is mounted approximately 1 m directly above the disk with the laser aimed at a patch of retroreflective tape on top of the steel disk. The forward propagation step uses a burst chirp broadcast from the Polytec generator with an amplitude of 0.5 V that is amplified by a Tabor (Nesher, Israel) 9400 high-voltage amplifier, with a 50 times gain, and is input to the piezoelectric transducer. To utilize the piezoelectric transducer efficiently, a chirp bandwidth of 75–125 kHz is chosen, centered on the transducer's primary radial resonance frequency, and is broadcast for the first half of a 51.2 ms period. A sampling frequency of 1280 kHz, with $N = 65\,536$ sample points, and a laser sensitivity of 25 mm/s/V is used. It was found that 30 averages sufficiently

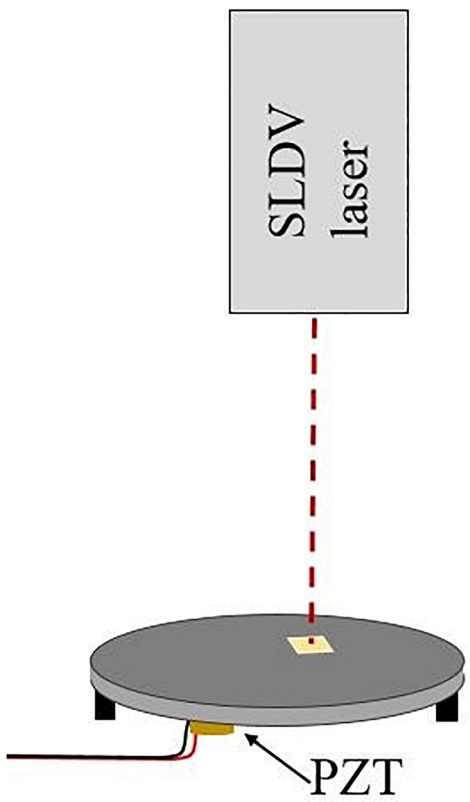

FIG. 2. (Color online) Experimental setup with scanning laser Doppler vibrometer (SLDV) pointed at a steel disk. The steel disk has a piezoelectric transducer (PZT) epoxied to the bottom.

reduced noise in the system allowing these settings to be used for both the forward and backward propagation steps. After the impulse response is measured it is normalized and reversed in time. Any additional signal processing techniques, such as one-bit or clipping TR, are then implemented and the resultant signal is broadcast into the steel disk, creating a focus at the location where the SLDV measured the impulse response.

In an additional experiment, a focus is generated at a single location on the steel disk for each of the signal processing techniques and the wave field is scanned with the SLDV. This gives a spatial map of the velocity at and around the focal location, allowing the spatial extent of the focus to be quantified. For these spatial scans, a region of the steel disk 72 mm × 60 mm in size is covered with retro-reflective tape and a scan grid of 51 points × 43 points is defined, giving a spatial resolution in each dimension of ∼1.4 mm. As reported by Young *et al.*[32] the average wavelength for these experiments is 26 mm, thus, the grid spacing is 0.54λ. A focus is generated at scan position (37,33.5) mm and the focus is repeated at this location as the SLDV measures the velocity at each scan position.

III. TR SIGNAL PROCESSING MODIFICATION TECHNIQUES

Deconvolution TR, or inverse filtering, is the first technique optimized to apply to the impulse response. Deconvolution TR inverts the spectrum of the impulse response such that when the resulting RIR is broadcast, the system resonances and antiresonances are compensated for in the backward propagation, yielding a focal signal with nearly a flat frequency response. In practice, deconvolution TR takes the spectrum of the impulse response, $R(\omega)^*$, where the "$*$" symbol denotes a complex conjugation, and normalizes it by its squared magnitude plus a scaling factor, γ, multiplied by the mean of the squared magnitude, as shown in

$$R_{\text{deconv}} = \frac{R(\omega)^*}{|R(\omega)|^2 + \gamma\,\text{mean}(|R(\omega)|^2)}. \tag{1}$$

The term $\gamma\,\text{mean}(|R(\omega)|^2)$ is a regularization term used to keep the deconvolution TR operation finite, a process described in more detail by Anderson *et al.*[23] Optimization of γ for reduction of the energy on either side of the peak focusing (termed side lobes[39]) followed the process described by Willardson *et al.*[21] and determined an optimal γ value of 0.9, which was also the value reported by Anderson *et al.* for TR focusing of waves in solid media.[23] As γ approaches infinity, the deconvolution TR process returns a traditional RIR because the γ term dominates in the denominator of Eq. (1) and after normalization, Eq. (1) returns $R(\omega)^*$. As γ approaches zero, the impulse response begins to look more like an impulse, effectively eliminating the reverberation in the impulse response. The modified RIR, after the deconvolution TR operation and with $\gamma = 0.9$, is shown in Fig. 3(b).

The one-bit TR technique alters the amplitude of the normalized RIR, $r(-t)$, according to the relationship of the instantaneous amplitude compared to a user-defined threshold [see Fig. 3(c)]. The threshold is applied at a positive value T_{OB} and at a negative value $-T_{\text{OB}}$. At time sample t_i, if $|r(-t_i)| \geq T_{\text{OB}}$, then $r(-t_i) \stackrel{\text{def}}{=} \text{sign}(r(-t_i))T_{\text{OB}}$. In other words, any signal above or below the positive or negative threshold, respectively, is set equal to the threshold (or the negative threshold), which is 0.2 in Fig. 3(d). If $|r(-t_i)| < T_{\text{OB}}$, then $r(-t_i) \stackrel{\text{def}}{=} 0$. The quantity $r(-t)$ is then normalized and the resulting modified impulse response is comprised of $+1,-1$, and 0 values, hence, the name one-bit TR [see Fig. 3(e)]. The purpose of one-bit TR is to amplify low-amplitude reflections in the impulse response and zero-out information with a poor SNR, but maintain the phase information of the non-zero signal. The threshold can be set anywhere from zero to one, thereby defining the acceptable SNR.

Clipping TR, a fairly new technique, is very similar to one-bit TR apart from one key difference.[40] A threshold, T_{CP}, is applied to the impulse response, just as with one-bit TR, and if $|r(-t_i)| \geq T_{\text{CP}}$, then $r(-t_i) \stackrel{\text{def}}{=} \text{sign}(r(-t_i))T_{\text{CP}}$. However, any signal below the threshold is not set equal to zero as with one-bit TR processing, and instead is unmodified [see Figs. 3(f) and 3(g) where threshold is 0.2]. When this resulting signal is normalized, any "clipped" signal is set to one and all of the signal that was below the threshold is amplified relative to the original normalized impulse response [see Fig. 3(h)]. Like one-bit TR, clipping TR amplifies later reflections, but it also amplifies all low-level signals in the recorded impulse response, potentially amplifying background noise.

Decay compensation TR attempts to compensate for the exponential decay of the impulse response.[20,21] As explained by Willardson *et al.*, the envelope of the RIR is obtained through a Hilbert transform operation, after which the envelope is smoothed through the use of a moving average filter [see Fig. 3(i)]. The envelope is inverted and normalized and then multiplied by the original, normalized RIR, point by point, creating a signal with approximately the same amplitude over all time [see Fig. 3(j)]. Because this can amplify unwanted noise, a threshold is applied with respect to the decay curve such that if the instantaneous value of the decay curve is below the threshold, the modified signal retains the values of the original, normalized RIR. An example signal after the decay compensation TR processing is shown in Fig. 3(k) with an applied threshold of 0.06.

Decay compensation implemented here, and in the work by Willardson *et al.*, compensated for the attenuation in the impulse response to produce a modified impulse response that essentially has a constant amplitude as a function of time. By contrast, the decay compensation implemented by Gliozzi *et al.* compensated for the attenuation in the impulse response twice, meaning that the inverted envelope is squared before multiplying by the impulse response. This means that the later arrivals of energy in the forward impulse response are made to be the largest amplitude portion of the modified RIR, and the early arrivals of energy and the direct sound are made to be the smallest amplitude portions of the modified RIR. The authors chose not to use the method of Gliozzi *et al.* since the SNR is the smallest in the latest arrivals of the impulse response and would therefore be amplified

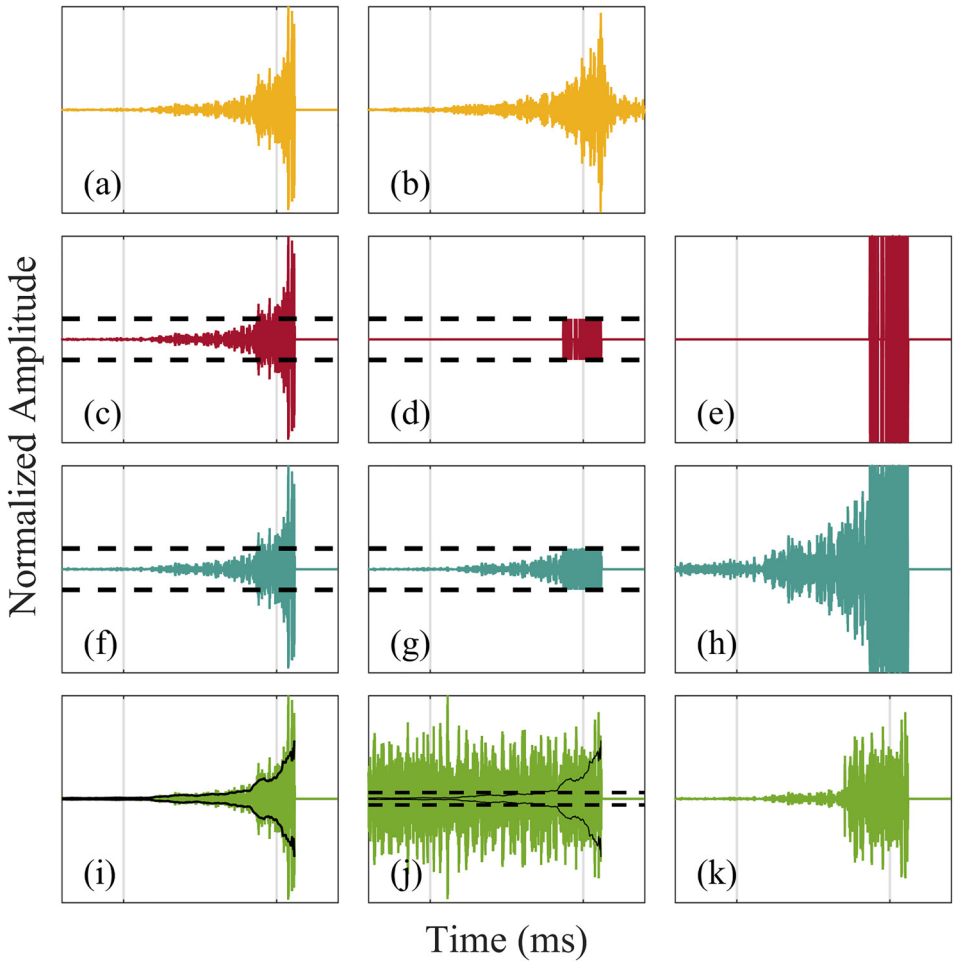

FIG. 3. (Color online) Impulse response modification techniques with each starting with a traditional RIR, (a),(b) deconvolution TR; (c)–(e) one-bit TR with a threshold of 0.2, indicated by the dashed black lines; (f)–(h) clipping TR with a threshold of 0.2; (i)–(k) decay compensation TR with a threshold of 0.06.

by the implementation suggested by Gliozzi *et al*. The decay compensation proposed by Willardson *et al*. maximizes the energy broadcast by the sources during the backward propagation step. Future work could compare the technique of Gliozzi *et al*. to the technique of Willardson *et al*. as was done in this paper.

It is important to point out that each of the modified RIR(s) are broadcast with the same peak amplitudes. In other words, the modified RIR(s) are normalized by their respective peak amplitudes prior to their broadcast. Thus, these modified RIR(s) are not broadcast with the same total energy from source transducers during the backward step. This normalization maximizes the output from the amplifier for a given amplification level. One of the main reasons why some of these modified RIR(s) achieve a higher peak amplitude in TR focusing is because more energy is broadcast as a result of the RIR modification.

IV. FOCAL SIGNAL ANALYSIS METRICS

Four primary metrics are used to quantify the relative merits of the focal signals generated by each of these impulse response modification techniques, three of which were introduced by Denison and Anderson.[41] The processing methods of deconvolution, one-bit, clipping, and decay compensation TR each result in changing more than just peak focal amplitude, and can often result in significant drawbacks along with their benefits. By applying quantitative measures to the focal signal, some of these drawbacks are identified, especially as related to adjustments in the threshold value used in each case. The first metric is the value of the peak amplitude in the time domain waveform at the location of the focus (the focal signal), called the peak focal amplitude, A_p. The second metric, called temporal quality, ξ_t, is a ratio of the instantaneous energy contained in A_p to the average energy in the entire focal signal, $A(x_0, y_0, t)$, of number of time samples N, at the focal location (x_0, y_0),

$$\xi_t = \sqrt{\frac{[A_p]^2}{\frac{1}{N}\sum_{n=1}^{N}\left[A(x_0, y_0, n)\right]^2}}. \tag{2}$$

A square root operation is used to express the ratio of these energy quantities as a ratio of amplitudes. While variations in the result for Eq. (2) can be obtained by using different time windows of the signal, for this study, the entire 51.2 ms signal was used. ξ_t illuminates characteristics of the focal signal otherwise only gleaned from a visual examination of time waveforms, such as the amplitude of the side lobes compared to A_p.

An additional temporal metric describing the symmetry of the focal signal, Σ, developed by Ulrich *et al*.[42] will be included in the analysis. Because the traditional TR process is inherently a symmetry process, the symmetry metric was developed to aid in the determination of the focal time and

the localization of a TR focus in space when plotting a symmetry map for several scan locations. This metric requires a cross correlation analysis of the left half (portion of the focal signal before the time of peak focusing) to the right half (portion of the focal signal after the time of peak focusing). A similar symmetry metric was developed by Gliozzi *et al.* that subtracts the left and right halves and sums the residual signal in the summation.[20]

Spatial quality, ξ_s, the third metric, defines a ratio of the energy in the peak focal amplitude, A_p, which occurs at the focal location, to the average energy of the spatial locations that surround it at the time of the focus, t_0,

$$\xi_s = \sqrt{\frac{[A_p]^2}{\frac{1}{M_x M_y}\sum_{m_x=1}^{M_x}\sum_{m_y=1}^{M_y}\left[A(m_x, m_y, t_0)\right]^2}}, \tag{3}$$

where M_x and M_y are the number of spatial locations sampled in the x and y directions, respectively.[40,41] The velocity at each point, $A(m_x, m_y, t)$, is measured as the TR process is repeated while the SLDV records the velocity at $M_x \times M_y$ spatial points both at and surrounding the focal location. At t_0, ξ_s represents how significant the peak amplitude is to the rest of the amplitude over the entire scan area. Given in conjunction with ξ_s are values for the full width at half-maximum (FWHM) values for the spatial extent of the focusing. The FWHM is determined from two cross-sectional plots of the instantaneous squared velocity along the x and y axes in the spatial map of the focusing to determine the full width of the focus at half the maximum amplitude.

The fourth metric examines the harmonic content of the spectrum of the focal signal (the focal spectrum) by quantifying a ratio of the energy contained in the fundamental frequency bandwidth (75–125 kHz), to the second (150–250 kHz) or third (225–375 kHz) harmonic frequency bandwidth. Because the chirp of the forward propagation step has a finite-bandwidth, the frequency content of the focal spectrum for traditional TR should be limited to the fundamental bandwidth. Any second or third harmonics of the fundamental bandwidth that occur can only be a result of nonlinearity in the system, whether that is the physical system or any nonlinear signal processing. Mathematically, the fundamental-to-second harmonic ratio, R_{12}, is

$$R_{12} = 10\log_{10}\left(\frac{\frac{1}{N_1}\sum_{f_0}^{f_1}|F|^2}{\frac{1}{N_2}\sum_{2f_0}^{2f_1}|F|^2}\right). \tag{4}$$

The absolute value of the square of the focal spectrum, $|F|^2$, is summed across the values between $f_0 = 75$ kHz and $f_1 = 125$ kHz, the fundamental bandwidth, then scaled by the number of points within that bandwidth, N_1. This quantity is divided by a similar term wherein $|F|^2$ has been summed across the values between $2f_0$ and $2f_1$, the second harmonic, and divided by N_2, the number of frequency points in the second harmonic. The fundamental-to-third harmonic ratio, R_{13}, is defined similarly,

$$R_{13} = 10\log_{10}\left(\frac{\frac{1}{N_1}\sum_{f_0}^{f_1}|F|^2}{\frac{1}{N_3}\sum_{3f_0}^{3f_1}|F|^2}\right). \tag{5}$$

V. RESULTS

In examining the focal signals, many of the benefits and drawbacks of these impulse response modification techniques are made manifest. Figure 4 shows five example focal signals. Each were measured at the same focal location using the same source chirp signal and hence start out with the same impulse response signal, but this impulse response was then processed with the five different signal processing modification techniques described in Sec. III. Figure 4(a) shows the focal signal generated using an unmodified impulse response, or traditional TR, where an impulse response is only flipped in time and broadcast to generate a focal signal. This focal signal has the expected symmetrical side lobes with a $A_p = 10$ mm/s and $\xi_t = 34.1$, and is the baseline against which all of the other focal signals are compared. The focal signal shown in Fig. 4(b) uses deconvolution TR and one may observe that, relative to traditional TR, the energy in the side lobes are reduced in the focal signal [shown in Fig. 4(b)], resulting in a signal that more closely approximates a delta function. This is confirmed by the ξ_t, which equals 60 for deconvolution TR; however, this benefit is obtained at the expense of a reduction in A_p to 5 mm/s, a factor of 2 relative to traditional TR. A one-bit TR focal signal is shown in Fig. 4(c) with $A_p = 30$ mm/s. This focal signal employed a threshold value of 0.02 to amplify the impulse response, which increases the A_p but also dramatically increases the amplitude of the side lobes prior to the focus, resulting in a non-symmetrical focal signal with $\xi_t = 24.2$. Even more non-symmetric side lobe amplitudes are evident in the clipping TR focal signal in Fig. 4(d) where $\xi_t = 22.2$. This focal signal also employs a threshold of 0.02 but is able to reach $A_p = 32$ mm/s. The focal signal displayed in Fig. 4(e) is generated with decay compensation TR also at a threshold of 0.02. The $A_p = 27$ mm/s here is not quite as high as that shown in Figs. 4(c) and 4(d), but the heavily asymmetric side lobes are just as evident, as indicated by $\xi_t = 22.5$.

A. Peak focal amplitude

As explained previously, the threshold used in the modification techniques of one-bit, clipping, and decay compensation TR can be defined as any number between zero and one, where a lower number ultimately boosts low-amplitude arrivals later in the impulse response relative to the higher amplitude arrivals earlier in the impulse response. This sends more energy overall into the medium, upon normalization of

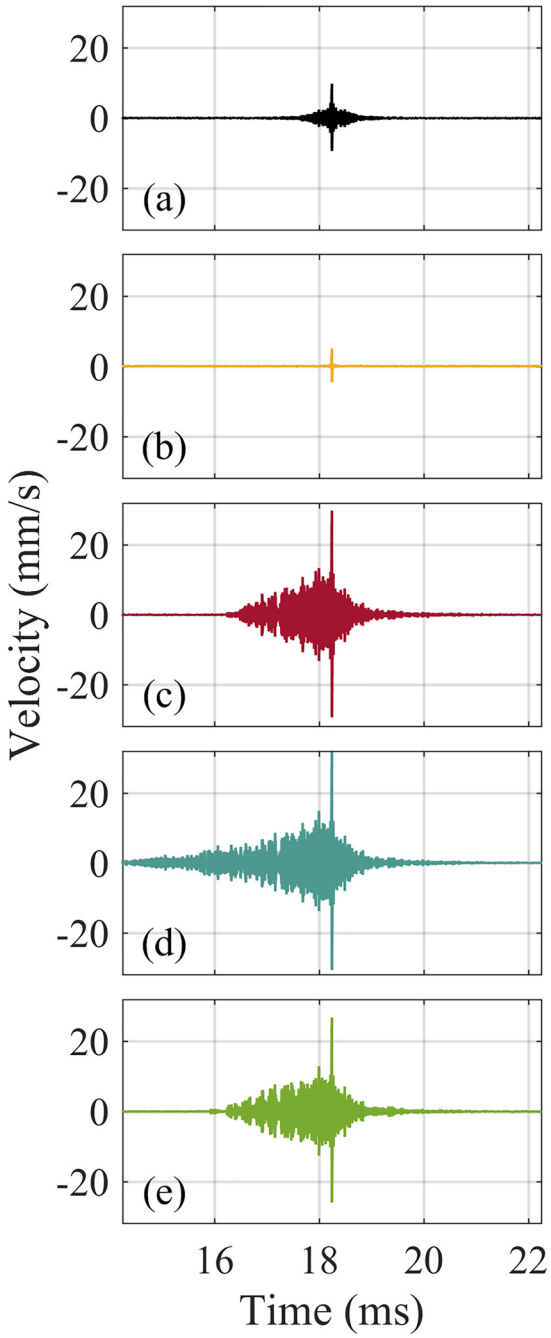

FIG. 4. (Color online) Measured focus signals using (a) traditional, (b) deconvolution, (c) one-bit, (d) clipping, and (e) decay compensation TR. One-bit, clipping, and decay compensation TR all use a threshold value of 0.02.

the reversed signal, which is then broadcast in the backward propagation step. Figure 5 reports the A_p measured from all five processing techniques versus the threshold applied. The A_p of traditional TR and deconvolution TR are plotted with a threshold value of one because they do not use a threshold in their processing but are worth comparing to. At the lowest thresholds shown, between 10^{-4} and 10^{-3}, the A_p of one-bit, clipping, and decay compensation TR all plateau at around 29 mm/s. At these thresholds, all of the coherent signal has been amplified during the impulse response processing and thus no further gains in A_p are possible. Though not shown, focal signals were actually obtained with thresholds as low

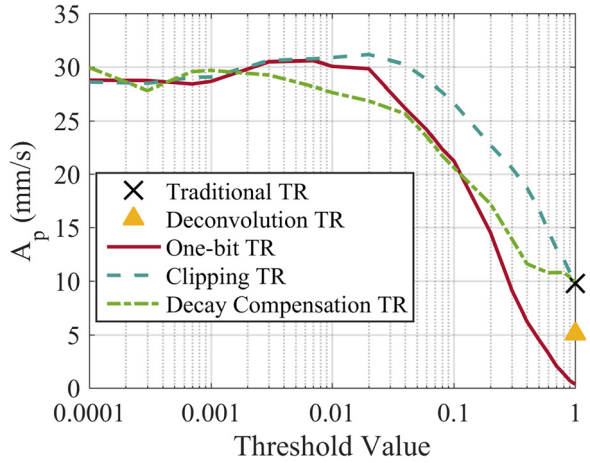

FIG. 5. (Color online) Peak focal amplitude, A_p, versus threshold applied obtained from TR focal signals with various TR processing techniques applied. Traditional TR and deconvolution TR do not use a threshold and so are plotted at a threshold of one.

as 10^{-12} and it was found that A_p did not increase beyond the 28–30 mm/s region. In the vicinity of a threshold value of 0.01, one-bit and clipping TR provide a maximal A_p. These maxima are likely a balance between amplifying late arrivals in the impulse response and amplifying background noise in the impulse response. Any noise that is amplified generates destructive interference while any amplified late reflections will constructively interfere in the TR focusing. On the contrary, the A_p of decay compensation TR is optimal only at the lowest threshold values and converges to traditional TR at a threshold of one. One-bit and clipping TR are maximized at thresholds of 0.007 and 0.02, respectively, with clipping TR reaching the highest overall peak focal amplitude of 31 mm/s. Both methods achieve lower A_p as the threshold is increased with clipping TR being equivalent to traditional TR at the limiting value of one and the A_p for one-bit TR going to zero. Clipping TR merges with traditional TR and one-bit TR does not at a threshold of one because these techniques treat the signal below the threshold differently. One-bit TR zeros out the signal below the threshold while clipping TR leaves it intact meaning that a threshold of one would leave one-bit TR with an impulse response of mostly zeros with a single sample value set to one. The resulting TR focal signal is not a focus at all but merely a low-amplitude impulse response. Clipping TR would return a traditional focal signal for a threshold of one. Decay compensation TR merges with traditional TR at a threshold of one for reasons similar to clipping TR.

B. Temporal quality

ξ_t was calculated for the focal signals obtained with a range of thresholds and is a second instructive way to study the impact of threshold for each method. The curves displayed in Fig. 6 show an overall increase in ξ_t with an increasing threshold, reaching an approximate maximum at a threshold value of one when the curves merge with traditional TR. This indicates that, aside from deconvolution TR, traditional TR has the lowest amplitude side lobes and therefore the cleanest focal signal. The application of a threshold

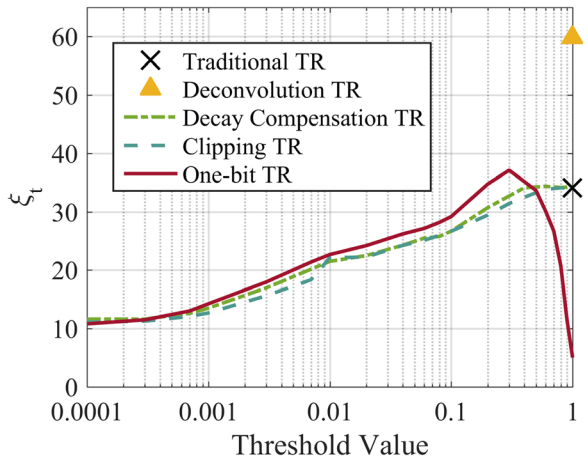

FIG. 6. (Color online) Temporal quality, ξ_t, versus threshold applied obtained from TR focal signals with various TR processing techniques applied. Traditional TR and deconvolution TR are plotted at a threshold value of one.

for one-bit, clipping, and decay compensation TR techniques results in an increase in the amplitude of side lobes in exchange for a gain in A_p. The notable exception is one-bit TR, which never collapses with traditional TR, as described in the previous paragraph, but instead drops sharply in ξ_t over thresholds from 0.3 to 1. The overarching trade-off presented by the threshold analysis is that a lower threshold results in higher A_p with a decrease in ξ_t. A high threshold results in a high ξ_t but lower A_p. The application of the TR processing is then what should determine whether maximal A_p or maximal ξ_t is more important. For crack detection in NDE, high A_p, whatever the processing used to obtain it, is assumed to be ideal for the excitation of nonlinear vibrations of a crack. While high ξ_t produces very clean signals, which is important for communications applications for example,[43] the accompanying low A_p likely makes it unsuitable for crack detection, and thus it will not be further explored. With this in mind the optimal threshold value for one-bit, clipping, and decay compensation TR techniques is suggested to be 0.02 to yield a high A_p while maintaining a reasonably high ξ_t.

Σ values are included in Table I for each of the focal signals. Traditional TR is determined to be the most symmetric process. The rest of the modification techniques have significantly lower Σ values. A quick glance at Fig. 4 illustrates why the focal signals generated by one-bit, clipping, and decay compensation TR techniques all provide lower Σ values since they all have larger amplitudes in the left half of the signal than in the right half of the signal. A value of $\Sigma = 1$ means that the left half and the right half are perfectly symmetric and identical to reversed versions of each other.

C. Spatial quality

ξ_s was calculated according to Eq. (3) using the spatial scans collected for each of the five signal processing techniques. Table I shows the results of this analysis where one-bit, clipping, and decay compensation TR are generated with thresholds of 0.02. In the first data column, ξ_s for decay compensation TR gives the highest value of 4.6, indicating

TABLE I. Symmetry, spatial quality, and full width at half-maximum (FWHM) of the spatial scans taken of a focal signal for each TR signal processing technique. A threshold of 0.02 was used for one-bit, clipping, and decay compensation TR techniques.

Technique	Σ	ξ_s	FWHM (mm)
Traditional TR	0.96	3.5	13.6
Deconvolution TR	0.81	3.9	12.6
One-bit TR	0.78	4.4	12.3
Clipping TR	0.70	4.3	12.8
Decay compensation TR	0.73	4.6	12.5

that decay compensation has the most energy in its peak focal value relative to the energy in the field around it. Each of the modification techniques yields a higher ξ_s than the value obtained for traditional TR. It is interesting that one-bit TR, clipping TR, and decay compensation TR all yield higher ξ_s values since the side lobes for each of these techniques are higher than obtained with traditional TR as observed in Fig. 6.

The FWHM is smaller for all techniques relative to traditional TR. This is not surprising for deconvolution TR since the purpose of this technique is to temporally and spatially compress the focus. The FWHMs for one-bit, clipping, and decay compensation TR are smaller than traditional TR, a somewhat surprising result, but helpful in this case since it shows that they do not increase the spatial extent of the focus. A larger focal size could decrease the resolution with which cracks can be detected, making crack detection less reliable overall. However, since this is not the case for any of the modification techniques shown here, the benefits to crack detection of a spatially compressed TR focus remain intact.

D. Harmonic generation

Because one-bit, clipping, and decay compensation TR utilize nonlinear processing of the RIR, an examination of the spectral content of the focal signals is vital. Nonlinear frequency content generated by the impulse response modification techniques effectively raises the noise floor in harmonic frequency bands, thereby decreasing the ability to detect harmonic generation in a focal signal. Focal spectra of the focal signals measured using one-bit, clipping, and decay compensation TR are shown in Figs. 7(b)–7(d), respectively. The threshold used for all three methods is 0.02, the same as the focal signals shown in Fig. 4, and is the optimal threshold value as determined in Secs. V A, V B, and V C. The focal spectrum created using traditional TR is helpful for comparison and is given in Fig. 7(a). In each plot in Fig. 7, the fundamental bandwidth is defined as the frequency content between the two solid vertical lines (75–125 kHz), the second harmonic bandwidth is between the two dashed vertical lines (150–250 kHz), and the third harmonic bandwidth is between the two dashed-dotted vertical lines (225–375 kHz). With these bandwidths defined, the amplitudes in each bandwidth may be compared. The fundamental bandwidth amplitude is clearly the lowest in traditional TR and the highest for clipping TR, which is expected given their peak focal amplitudes. For the second and third harmonics, this is not

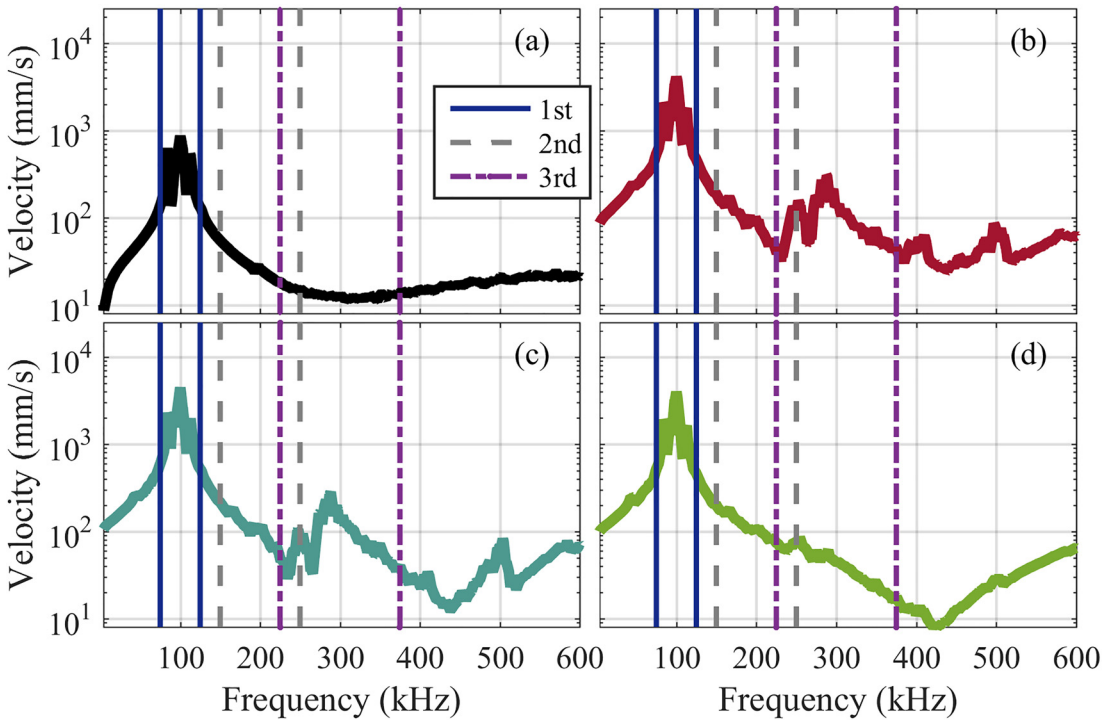

FIG. 7. (Color online) The focal spectra measured with (a) traditional TR, (b) one-bit TR, (c) clipping TR, (d) decay compensation TR. (b)–(d) use a threshold of 0.02 for the impulse response modification. The region between the solid vertical lines is the fundamental bandwidth (75–125 kHz). The region between the dashed lines is the second harmonic (150–250 kHz), and the region between the dashed-dotted lines is the third harmonic (225–375 kHz).

true. Traditional TR appears to contain only uncorrelated background noise in the harmonic bandwidths, increasing somewhat with frequency above 300 kHz. Both clipping and one-bit TR spectra exhibit a marked increase in harmonic amplitudes, especially for the third harmonic. In fact, both clipping and one-bit TR exhibit increases in the fifth harmonic amplitudes as well. Decay compensation TR does exhibit an increase in harmonic content, but this introduction of higher frequency content decreases as frequency increases (until 425 kHz) and the levels of the harmonic amplitudes are at least half as high as in clipping and one-bit TR. All three techniques are nonlinear processes but clearly the other two are more nonlinear than decay compensation TR.

On closer examination of the higher frequency spectra of clipping and one-bit TR, the marked increases in harmonic amplitudes centered about 300 and 500 kHz represent odd harmonics of the fundamental peak centered about 100 kHz. This is because the two techniques essentially create square waves, which have prominent odd harmonics. Decay compensation TR does not alter the waveform structure as dramatically; so, while decay compensation TR does generate some increase in harmonic amplitudes, it is not nearly as prominent as the increases introduced by clipping and one-bit TR.

To better quantify the harmonic content, ratios between the first harmonic and the second or third harmonic bandwidths can be calculated using Eqs. (4) and (5). The results of these calculations are shown in Table II. The best case scenario for a harmonic ratio is traditional TR, which only has background noise at the harmonic frequencies, and so has the largest ratios of $R_{12} = 37$ dB and $R_{13} = 34$ dB. The next best is decay compensation TR, which has a lower $R_{12} = 35$ dB, but an equal $R_{13} = 34$ dB. It is clear in Fig. 7 that the amplitude of the third harmonic is higher for decay compensation TR than for traditional TR, but the fundamental amplitude also is markedly higher for decay compensation TR than for traditional TR. The ratios for clipping and one-bit TR are lower, especially for R_{13}, for the reasons identified in the previous paragraph. It should be remembered that when a crack vibrates it does so nonlinearly and thus a higher amplitude excitation raises the harmonic frequency amplitudes by more than any increase in the fundamental frequency amplitude. Hence, while these modification techniques have lower fundamental to higher harmonic amplitude ratios, they each should be able to induce a larger nonlinear response of a crack.

VI. NONLINEAR DETECTION OF SCC USING DECAY COMPENSATION TR

Because decay compensation TR has shown to provide higher A_p without a significant decrease in R_{12} and R_{13}, a preliminary study was conducted for nonlinear TR crack detection using decay compensation TR as the means of excitation

TABLE II. Harmonic ratios: The ratio of the energy in the fundamental bandwidth to the energy in a higher harmonic, shown below for the second harmonic, R_{12}, and the third harmonic, R_{13} for each of the amplitude-increasing modification techniques and traditional TR.

Technique	R_{12} (dB)	R_{13} (dB)
Traditional TR	37	34
One-bit TR	30	24
Clipping TR	33	26
Decay compensation TR	35	34

to detect SCC. SCC is known to develop in steel in the heat-affected-zone surrounding welds that are exposed to harsh environments.[44] To obtain a sample with SCC, a 304 L steel rod, 12.7 cm (5 in.) in length and 1.59 cm (5/8 in.) in diameter, is cut in half and welded back together. The sample is then exposed to a 42% magnesium chloride bath at a temperature of 80 °C for 12 days, following recommendations of Jackson *et al.*[45] The creation of these damaged samples was described by Hogg *et al.*[46] and Young *et al.*[32] After exposure the rod is epoxied to the top of the disk used in the previous study and to the bottom of the disk are epoxied eight piezoelectric transducers (APC, material type 850, Mackeyville, PA) with diameter 19 mm and thickness 12 mm. The piezoelectric transducers are connected to two four-channel, 50× gain, Tabor 9400 amplifiers (Nesher, Israel) that, in turn, are connected to a National Instruments (Austin, TX) PXI-7852R eight-channel generator card. A SLDV, externally controlled by custom LabVIEW-based software (Austin, TX), is directed to scan 200 points along a 50 mm length of the rod (0.25 mm spacing between scan points), extending roughly 20 mm to either side of the edge of the weld. For each scan point, each of the eight generation channels, in turn, emits a 2 V, 75–125 kHz chirp signal, and each of the chirp responses are measured at the current scan point with the SLDV. Eight RIRs are calculated using either traditional TR or decay compensation TR, and simultaneously emitted from the piezoelectric transducers at 0.25 V and then again at 1.5 V. A TR focus of energy is generated by each transducer and the simultaneous emission of all eight transducers ensures that these foci superpose at the scan location. The SLDV has a sensitivity of 25 mm/s/V and the signal is acquired with a National Instruments PXIe-5122 Digitizer with 14-bit resolution. In a previous study Young *et al.*[32] used this sample and others like it to determine that the amplitude of the second harmonic generally increased with longer exposure to the magnesium chloride bath as described previously due to the increasing amount of SCC in the rods.

At each scan location, it is possible to calculate the nonlinearity present in the focal signal recorded at that location. First a spectrum of the entire focal signal, $G(f)$, is calculated. In order to compare relative increases in the amplitude of the second harmonic amplitude relative to the fundamental frequency amplitude, $G(f)$ may be scaled according to the Euclidean norm of the values contained within the fundamental bandwidth, where

$$\|G(f)\| = \frac{G(f)}{\sqrt{\sum_{75\,\mathrm{kHz}}^{125\,\mathrm{kHz}} G^2(f)}}. \tag{6}$$

As suggested by Young *et al.*[32] a nonlinearity parameter, ζ, which is essentially a scaled version of the ratio of the second harmonic amplitude to the fundamental frequency amplitude, may then be calculated

$$\zeta = \sum_{150\,\mathrm{kHz}}^{250\,\mathrm{kHz}} \|G(x,\theta_n,f)\|^2. \tag{7}$$

The detection ability of decay compensation TR can be directly compared to that of traditional TR, point by point, in Fig. 8 with ζ plotted versus distance along the bar length. Note that the angle at which these data were taken corresponds to the 180° angle for this bar as described in Young *et al.*,[32] and the traditional TR data shown here in Fig. 8(b) correspond to the data shown in Fig. 8(c) of that paper.

Given the propensity to damage formation in the heat-affected-zone, second harmonic nonlinearity is expected to increase in the assumed heat-affected-zone regions spanning 9–19 mm and 30–40 mm on either side of the weld. Two vertical dashed lines at 19 mm and 30 mm give the approximate location of the outer edge of the weld, meaning the material between 19 and 30 mm is comprised of the weld itself. In Fig. 8(a), where a 0.25 V excitation was used, the most notable distinction between the two techniques is that traditional TR presents higher values of normalized nonlinearity than decay compensation TR at various locations. Both techniques exhibit features near 1, 10, 17, 30, 33, and 44 mm. The peaks at 10, 17, 30, and 33 are within the expected region for SCC to appear. However, the entire surface of this rod was exposed to a corrosive bath for 12 days and cracking can appear at any point along the bar, which is why Young *et al.*[32] suggested summing ζ across the length of the inspection region to get a single value representing the cumulative damage in the bar. The traditional TR data are more prone to noisy spikes in the data, most notably seen at 10.25, 18.75, 29.25, 30.75, 33.75, 41.75, and 42.5 mm, whereas the decay compensation TR has a noisy spike only at 45.5 mm. The data in Fig. 8(b) utilized a 1.5 V excitation with the same two TR techniques as used for the 0.25 V excitation. Neither of these data sets has large noisy spikes and, generally, both techniques exhibit features at the same locations as did the low-amplitude excitation. The noisy spikes in the plot of ζ using traditional TR with a low excitation amplitude again represent potential false detections of nonlinearity in the sample. One would expect that the higher amplitude excitation would yield more reliable detection of nonlinearities because the SNR at the second harmonic range of frequencies should improve with high-amplitude fundamental frequency excitation.

It is not possible at this time to know which technique yields the most correct imaging of the nonlinear features in the bar since the bar has not been destructively analyzed to locate SCC yet. However, we can compare the relative amplitudes of the features detected by each of the techniques at the two different excitation levels. The data in Fig. 8 may be normalized to the amplitude of the feature at 17 mm, shown in Fig. 9. The traditional TR data at low and high excitations are fairly similar to each other, aside from the noisy spikes in the low-amplitude excitation data and an amplitude difference of 1.6 for the feature at 10 mm. The decay compensation data at the two excitation levels [Fig. 9(b)] also compare well to each other, except at 1, 10, and 44 mm. The features at 1 and 44 mm are both lower in relative amplitude with the higher amplitude excitation, whereas the feature at 10 mm appears to merge with the larger feature at 17 mm (no trough between the features at 10 and 17 mm).

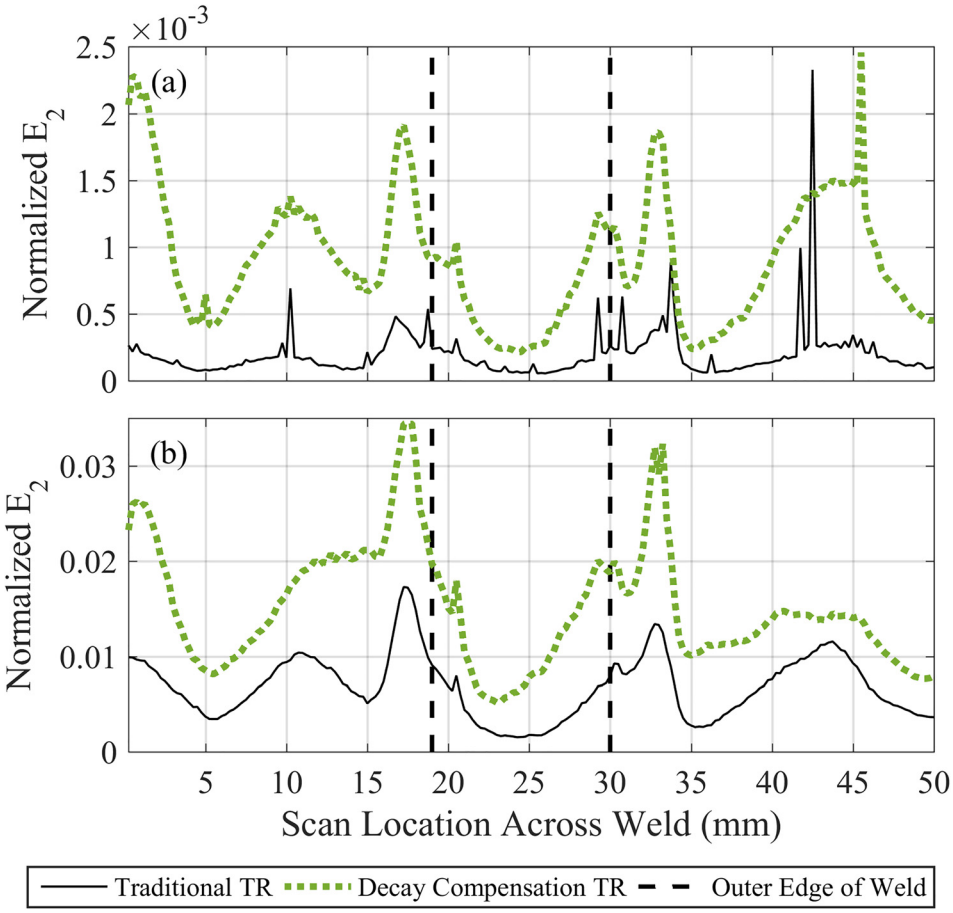

FIG. 8. (Color online) Nonlinearity parameter, ζ, contained in the focal signals obtained at each of the 200 scan locations along a rod with SCC. Traditional TR (black) and decay compensation TR (dotted) were used to excite TR foci at each location. (a) shows the results for an excitation amplitude of 0.25 V, while (b) shows the results for an excitation amplitude of 1.5 V. While ultimately unknown, SCC is likely to occur in the region just outside the weld on the rod, called the heat-affected-zone.

The features at 10, 17, 30, and 33 mm are all within the expected region for SCC to exist, and thus we can assume that they are accurate detections of SCC. The features at 1 and 44 mm, on the other hand, are outside of the regions of expected SCC and may be less likely to represent actual damage. The traditional TR data at both excitation levels have smaller ζ values than either of the decay compensation data sets. Therefore, if the features at 1 and 44 mm are not actually due to SCC then the traditional TR technique can be seen to be better, but it is hard to say whether those features are due to SCC or not until further analysis is conducted.

In practical implementations of TR for nonlinear NDE, it is always best to use the most robust technique that allows for the most reliable detection of defects. In a laboratory setting, one may be able to supply enough amplification and have a low enough background noise to comfortably use traditional TR. However, in practical implementations the noise floor is generally higher than in laboratory measurements due to increases in background noise, or if one is using a laser Doppler vibrometer they may be limited in the application of reflective tape to the sample under test.

VII. CONCLUSION

TR focusing used for the purpose of exciting nonlinearity in cracks has the potential to suffer from a low SNR and therefore false detections if only traditional TR techniques are utilized. Modifications to the RIR, wherein later reflections are amplified relative to early reflections, ultimately increase the peak focal amplitude, but often at the expense of lowering the temporal quality of the focal signal and increasing higher-order harmonics, a problem for nonlinear crack detection that relies on higher-order harmonics to sense cracks. Four techniques were studied relative to traditional TR: deconvolution, one-bit, clipping, and decay compensation TR. One-bit, clipping, and decay compensation TR were able to realize focal amplitudes three times higher than traditional TR. Deconvolution TR had a temporal quality much higher than any other technique, but with a focal amplitude that was much lower. Only decay compensation TR significantly increased peak focal amplitude without a drastic increase in higher harmonic content as well. In addition, spatial focus quality and the width of the focusing were found to be slightly better for the four modification techniques than for traditional TR. In the study of TR optimization in a reverberation chamber, Willardson *et al.* found results similar to these, but with clipping TR able to reach amplitudes over four times higher than traditional TR at a threshold value of 0.03.

Decay compensation TR was utilized to locate regions of high nonlinearity on a rod with SCC. These were then compared to results from the same test conducted using traditional TR. It was determined that, because of decay compensation TR's higher SNR in its focal signals, it was able to more cleanly detect nonlinearity compared to traditional TR. In addition, when the experiments were repeated at higher excitation amplitudes, the random spikes in nonlinearity disappeared.

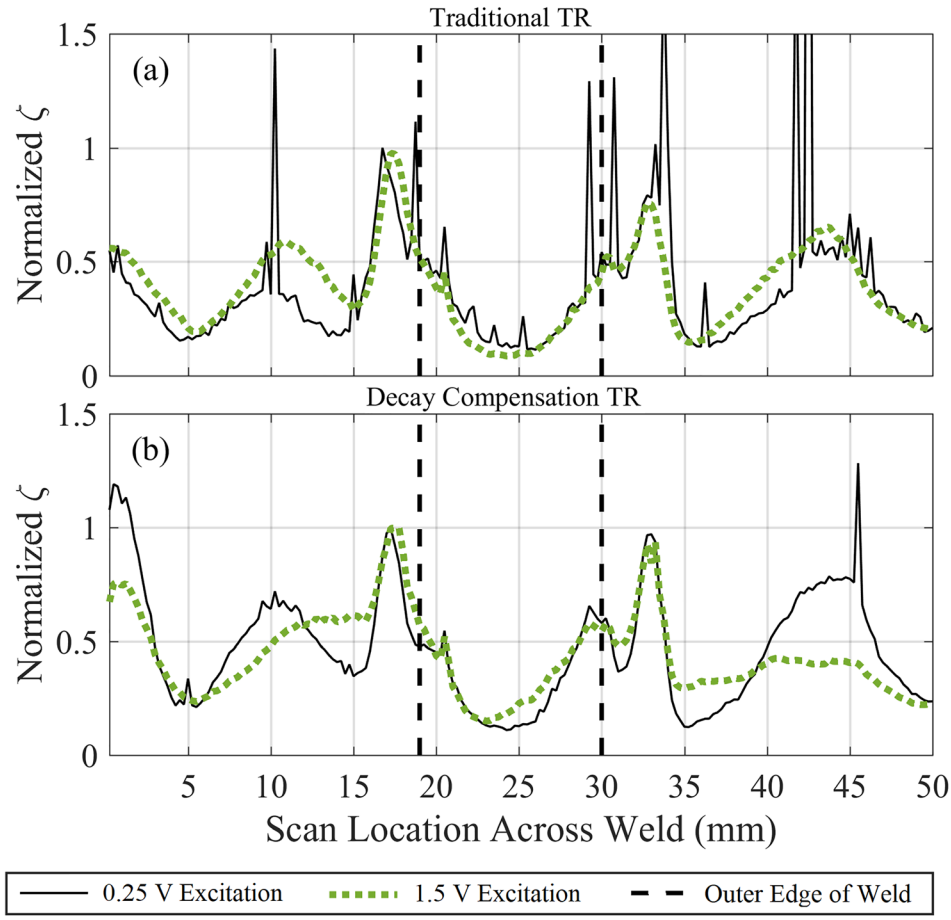

FIG. 9. (Color online) Normalized nonlinearity parameter, ζ, contained in the second harmonic of a focal signal obtained at each of the 200 scan locations along a rod with SCC. Traditional TR and decay compensation TR were used to excite TR foci at each location with excitation amplitudes of 0.25 V (solid lines) and 1.5 V (dotted lines). (a) shows the results for an excitation amplitude of 0.25 V, while (b) shows the results for an excitation amplitude of 1.5 V. The normalization of ζ is with respect to the respective values at 17 mm.

One of the major implications of this study is that a well-known technique such as one-bit TR, a technique used by many researchers to increase the focal amplitude of TR, introduces so much harmonic energy into the focal signal that it actually may become harder to detect a crack or defect in a sample, despite the increase in the focal amplitude. Thus, modifications to the impulse response to increase the focal amplitude may themselves introduce nonlinear distortions into the TR focusing because of the nonlinearities inherent in the signal processing used to modify the RIR(s). As mentioned in the Introduction, there are many techniques that have been developed to quantify the amount of distortion at a defect location that we expect will be impacted by these findings as well. Future work could explore how each of these specific nonlinearity detection techniques are impacted by the impulse response modifications.

ACKNOWLEDGMENTS

Funding was provided by the U.S. Department of Energy, Nuclear Energy University Program through Integrated Research Project Award No. DE-NE0008442, and a subcontract from Los Alamos National Laboratory to Brigham Young University (BYU). Additional support provided by the BYU College of Physical and Mathematical Sciences.

[1]M. Fink, "Time reversed acoustics," Phys. Today **50**(3), 34–40 (1997).
[2]B. E. Anderson, M. Griffa, C. Larmat, T. J. Ulrich, and P. A. Johnson, "Time reversal," Acoust. Today **4**(1), 5–16 (2008).
[3]N. Chakroun, M. Fink, and F. Wu, "Time reversal processing in ultrasonic nondestructive testing," IEEE Trans. Ultrason. Ferroelectr. Freq. Control **42**, 1087–1098 (1995).
[4]V. Miette, L. Sandrin, F. Wu, and M. Fink, "Optimisation of time reversal processing in titanium inspections," in *Proceedings of the 1996 IEEE Ultrasonics Symposium*, San Antonio, TX (November 3–6, 1996), pp. 643–647.
[5]R. Guyer, "Nonlinear tomography and time reversed acoustics," in *The 6th International Workshop on Nonlinear Elasticity in Materials*, Leuven, Belgium (2001).
[6]T. J. Ulrich, P. A. Johnson, and A. Sutin, "Imaging nonlinear scatterers applying the time reversal mirror," J. Acoust. Soc. Am. **119**(3), 1514–1518 (2006).
[7]T. J. Ulrich, P. A. Johnson, and R. A. Guyer, "Interaction dynamics of elastic waves with a complex nonlinear scatterer through the use of a time reversal mirror," Phys. Rev. Lett. **98**, 104301 (2007).
[8]B. E. Anderson, L. Pieczonka, M. C. Remillieux, T. J. Ulrich, and P.-Y. Le Bas, "Stress corrosion crack depth investigation using the time reversed elastic nonlinearity diagnostic," J. Acoust. Soc. Am. **141**(1), EL76–EL81 (2017).
[9]G. Zumpano and M. Meo, "A new nonlinear elastic time reversal acoustic method for the identification and localisation of stress corrosion cracking in welded plate-like structures—A simulation study," Int. J. Solids Struct. **44**(11), 3666–3684 (2007).
[10]B. E. Anderson, M. Griffa, T. J. Ulrich, P.-Y. Le Bas, R. A. Guyer, and P. A. Johnson, "Crack localization and characterization in solid media using time reversal techniques," in *Proceedings of the 44th U.S. Rock Mechanics Symposium and 5th U.S.-Canada Rock Mechanics Symposium*, Salt Lake City, UT (June 27–30, 2010), Paper No. 10-154.
[11]T. J. Ulrich, A. M. Sutin, T. Claytor, P. Papin, P.-Y. Le Bas, and J. A. TenCate, "The time reversed elastic nonlinearity diagnostic applied to evaluation of diffusion bonds," Appl. Phys. Lett. **93**(15), 151914 (2008).
[12]P.-Y. Le Bas, T. J. Ulrich, B. E. Anderson, R. A. Guyer, and P. A. Johnson, "Probing the interior of a solid volume with time reversal and nonlinear elastic wave spectroscopy," J. Acoust. Soc. Am. **130**(4), EL258–EL263 (2011).
[13]R. A. Guyer and P. A. Johnson, "Nonlinear mesoscopic elasticity: Evidence for a new class of materials," Phys. Today **52**(4), 30–35 (1999).

[14]P. A. Johnson, "The new wave in acoustic testing," Mat. World **7**, 544–546 (1999).
[15]P. B. Nagy, "Fatigue damage assessment by nonlinear ultrasonic materials characterization," Ultrasonics **36**, 375–381 (1998).
[16]M. Bentahar, R. El Guerjouma, S. Idijmarene, and M. Scalerandi, "Influence of noise on the threshold for detection of elastic nonlinearity," J. Appl. Phys. **113**, 043516 (2013).
[17]B. E. Anderson, M. C. Remillieux, P.-Y. Le Bas, and T. J. Ulrich, "Time reversal techniques," in *Nonlinear Acoustic Techniques for Nondestructive Evaluation*, 1st ed., edited by T. Kundu (Springer and Acoustical Society of America, Cham, Switzerland, 2018), Chap. 14, pp. 547–581.
[18]A. Derode, A. Tourin, and M. Fink, "Ultrasonic pulse compression with one-bit time reversal through multiple scattering," J. Appl. Phys. **85**(9), 6343–6352 (1999).
[19]G. Montaldo, P. Roux, A. Derode, C. Negreira, and M. Fink, "Generation of very high pressure pulses with 1-bit time reversal in a solid waveguide," J. Acoust. Soc. Am. **110**(6), 2849–2857 (2001).
[20]A. S. Gliozzi, M. Scalerandi, and P. Antonaci, "One-channel time-reversal acoustics in highly attenuating media," J. Phys. D: Appl. Phys. **46**, 135502 (2013).
[21]M. L. Willardson, B. E. Anderson, S. M. Young, M. H. Denison, and B. D. Patchett, "Time reversal focusing of high amplitude sound in a reverberation chamber," J. Acoust. Soc. Am. **143**(2), 696–705 (2018).
[22]M. Tanter, J.-L. Thomas, and M. Fink, "Time reversal and the inverse filter," J. Acoust. Soc. Am. **108**(1), 223–234 (2000).
[23]B. E. Anderson, J. Douma, T. J. Ulrich, and R. Snieder, "Improving spatio-temporal focusing and source reconstruction through deconvolution," Wave Motion **52**(9), 151–159 (2015).
[24]G. Ribay, J. de Rosny, and M. Fink, "Time reversal of noise sources in a reverberation room," J. Acoust. Soc. Am. **117**(5), 2866–28720 (2005).
[25]K. J. Haworth, J. B. Fowldes, P. L. Carson, and O. D. Kripfgans, "Generalized shot noise model for time-reversal in multiple-scattering media allowing for arbitrary inputs and windowing," J. Acoust. Soc. Am. **125**(5), 3129–3140 (2009).
[26]M. Davy, J. de Rosny, J.-C. Joly, and M. Fink, "Focusing and amplification of electromagnetic waves by time reversal in an leaky reverberation chamber," C. R. Phys. **11**, 37–43 (2010).
[27]O. Bou Matar, Y. F. Li, and K. Van Den Abeele, "On the use of a chaotic cavity transducer in nonlinear elastic imaging," Appl. Phys. Lett. **95**, 141913 (2009).
[28]O. Bou Matar, Y. Li, S. Delrue, and K. Van Den Abeele, "Optimization of chaotic cavity transducers to nonlinear elastic imaging," in *Proceedings of the 10th French Congress on Acoustics*, Lyon (2010).
[29]S. Delrue, K. Van Den Abeele, and O. Bou Matar, "Simulation study of a chaotic cavity transducer based virtual phased array used for focusing in the bulk of a solid material," Ultrasonics. **67**, 151–159 (2016).
[30]J. Robin, M. Tanter, and M. Pernot, "A semi-analytical model of a time reversal cavity for high-amplitude focused ultrasound applications," Phys. Med. Biol. **62**, 7471–7481 (2017).
[31]A. S. Gliozzi, M. Miniaci, F. Bosia, N. M. Pugno, and M. Scalerandi, "Metamaterials-based sensor to detect and locate nonlinear elastic sources," Appl. Phys. Lett. **107**, 161902 (2015).
[32]S. M. Young, B. E. Anderson, S. M. Hogg, P.-Y. Le Bas, and M. C. Remillieux, "Nonlinearity from stress corrosion cracking as a function of chloride exposure time using the time reversed elastic nonlinearity diagnostic," J. Acoust. Soc. Am. **145**(1), 382–391 (2019).
[33]F. Ciampa and M. Meo, "Nonlinear elastic imaging using reciprocal time reversal and third order symmetry analysis," J. Acoust. Soc. Am. **131**(6), 4316–4323 (2012).
[34]M. Scalerandi, A. S. Gliozzi, C. L. E. Bruno, D. Masera, and P. Bocca, "A scaling method to enhance detection of a nonlinear elastic response," Appl. Phys. Lett. **92**(10), 101912 (2008).
[35]M. Scalerandi, A. S. Gliozzi, C. L. E. Bruno, and K. Van Den Abeele, "Nonlinear acoustic time reversal imaging using the scaling subtraction method," J. Phys. D: Appl. Phys. **41**(21), 215404 (2008).
[36]P.-Y. Le Bas, M. C. Remillieux, L. Pieczonka, J. A. Ten Cate, B. E. Anderson, and T. J. Ulrich, "Damage imaging in a laminated composite plate using an air-coupled time reversal mirror," Appl. Phys. Lett. **107**, 184102 (2015).
[37]B. Van Damme, K. Van Den Abeele, Y. Li, and O. Bou Matar, "Time reversed acoustics techniques for elastic imaging in reverberant and nonreverberant media: An experimental study of the chaotic cavity transducer concept," J. Appl. Phys. **109**, 104910 (2011).
[38]B. E. Anderson, M. Clemens, and M. L. Willardson, "The effect of transducer directionality on time reversal focusing," J. Acoust. Soc. Am. **142**(1), EL95–El101 (2017).
[39]C. Draeger, J-C. Aime, and M. Fink, "One-channel time reversal in chaotic cavities: Experimental results," J. Acoust. Soc. Am. **105**(2), 618–625 (1999).
[40]C. Heaton, B. E. Anderson, and S. M. Young, "Time reversal focusing of elastic waves in plates for educational demonstration purposes," J. Acoust. Soc. Am. **141**(2), 1084–1092 (2017).
[41]M. H. Denison and B. E. Anderson, "Time reversal acoustics applied to rooms of various reverberation times," J. Acoust. Soc. Am. **144**(6), 3055–3066 (2018).
[42]T. J. Ulrich, M. Griffa, and B. E. Anderson, "Symmetry-based imaging condition in time reversed acoustics," J. Appl. Phys. **104**, 064912 (2008).
[43]B. E. Anderson, T. J. Ulrich, P.-Y. Le Bas, and J. A. Ten Cate, "Three-dimensional time reversal communications in elastic media," J. Acoust. Soc. Am. **139**(2), EL25–EL30 (2016).
[44]E. Gray, "Coast to coast spent fuel dry storage problems and recommendations," in *Division of Spent Fuel Management Regulatory Conference* (Nov. 2015), available at http://www.nrc.gov/public-involve/conference-symposia/dsfm/2015/dsfm-2015-erica-gray.pdf (Last viewed May 23, 2019).
[45]B. K. Jackson, D. A. Bosko, M. T. Cronin, J. L. W. Warwick, and J. J. Wall, "Detection of incipient SCC damage in primary loop piping using fiber optic strain gages," in *ASME Proc. Pressure Vessels and Piping*, PVP2014-28979 (2014).
[46]S. M. Hogg, B. E. Anderson, P.-Y. Le Bas, and M. C. Remillieux, "Nonlinear resonant ultrasound spectroscopy of stress corrosion cracking in stainless steel rods," NDT&E Int. **102**, 194–198 (2019).